

The characteristics of open cavity flow with a length to depth ratio of 4

Y. Y. Pey¹, L. P. Chua¹ & W. L. Siau²

¹*Department of Mechanical and Aerospace Engineering,
Nanyang Technological University, Singapore*

²*DSO National Laboratories, Singapore*

Abstract

The objective of this study is to characterize the flow behavior of an internal cavity of $L/D=4$, with its shear layer separated from a thick boundary layer at a free stream velocity of 15m/s. The study includes examining the cavity surface pressure and the associated flow structures. Pressure measurements were acquired from the cavity walls and the associated internal flow structures were studied using Particle Image Velocimetry (PIV). Several data processing techniques to study the flow structures were performed on the PIV data. These include time averaging quantities: velocities, vorticity and spatial correlation. In order to estimate the dynamics of the flow, the Proper Orthogonal Decomposition (POD) was applied to 900 independent PIV acquired velocities data set. The cavity wall surface pressure distribution indicated an open flow structure and was consistent with the mean velocity measurements which indicated a large re-circulating region within the cavity. Shear layer velocity profiles across the cavity revealed self-similarity beyond a distance of $x/L=0.3$. The shear layer growth rate of $d\theta/dx=0.031$ was close to the entrainment rate of a turbulent mixing layer, $d\theta/dx=0.035$. Two point spatial correlation coefficients of velocity fluctuations revealed a distinct pattern of alternating regions of positive and negative coefficient values, indicating the presence of organized coherent structures within the cavity. The modes one and two of the POD extracted structures indicated a flow structure of the closed cavity type. Mode three indicated the possibility of a large structure ejecting from the aft of the cavity.

Keywords: open cavity, coherent structures, proper orthogonal decomposition, particle image velocimetry, spatial correlation, self-similarity, recirculation.



1 Introduction

Study of flow over cavities is motivated by its phenomena found in many areas such as in solar cells, slots between movable parts of ships, tandem arrangements of bluff bodies such as adjacent tall buildings or tractor-trailer combinations, gas dynamic lasers, hydraulic gates, control valves, landing gears of aircrafts, sunroofs or windows in automobiles [1, 2]. Though geometrically simple, these cavities are associated with complex phenomenon. When exposed to free stream, the cavities experience unsteady flow around them. According to Rockwell *et al* [3], aero acoustic tones are not present at low speed (Mach number less than 0.3); thus, unsteady flow behaviors are due to inherent interaction of the free stream fluid with the lower speed fluid within the cavity. Cavities flow in general can be defined as open, closed or transitional. In open cavity, the flow separates at the leading edge of cavity and spans the entire length of the cavity. For a closed cavity, the flow reattaches on the cavity floor downstream of the leading edge before separating again near the downstream edge. A schematic diagram depicting typical flow in open and closed cavity is shown in Figure 1. In the case of transitional cavity flow, the separated shear layer attaches close to the aft of the cavity.

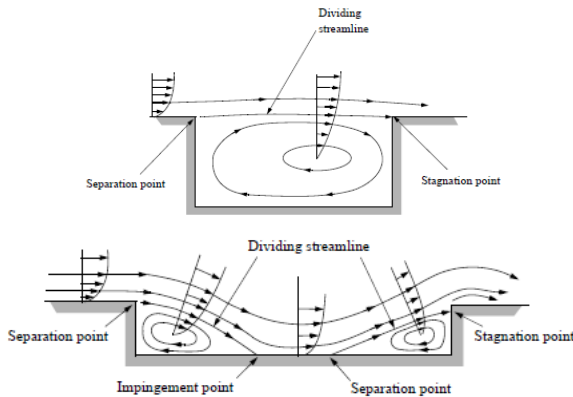


Figure 1: Schematic diagram of open cavity (left) and closed cavity (right) [4].

The current study was carried out on an open cavity with a length to depth ratio (L/D) of 4 at free stream velocity of 15m/s. It includes the measurement of pressure on cavity walls and the study of cavity internal flow structures through the use of Particle Image Velocimetry (PIV). Focus will be placed on investigating Reynolds stresses and coherent structures that develops within the cavity.

2 Experimental details

The experiments were carried out in an open loop wind tunnel with test section size of 220cm (length) by 40cm (width) by 40cm (height). The turbulence

intensity of the empty wind tunnel is about 1% at 30m/s. Operating speed of tunnel varies from 0m/s to 30m/s. The wind tunnel is represented schematically in Figure 2. The length of the cavity model is adjustable; L/D of 4 is used. Figure 3 shows the dimensions of the cavity structure. The cavity floor was instrumented with taps for pressure measurements along the centerline of the cavity floor. The width of the cavity spans the entire test section. The origin is taken to be at the leading edge of the cavity and at the middle of the cavity span.

The PIV system used consists of a double pulsed Nd:YAG laser, a HiSense MkII (Dantec Dynamics) camera and a system hub (FlowMap). The time between the laser pulses was set to be 50 μ s. The two images, captured during the laser pulses, were adaptive correlated successively starting from an initial interrogation window size of 64 by 64 pixels to a final size of 16 by 16 pixels with a 50% overlap ratio. A total of 900 time-independent images were captured in this study. The position of the PIV laser sheet is shown in Figure 4. The plane of interest lies on the x-y plane along the centreline of the cavity.

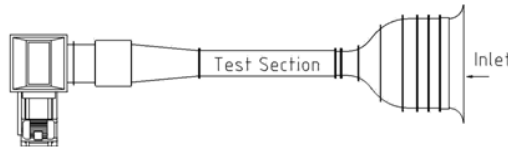


Figure 2: Schematic diagram of wind tunnel top view.

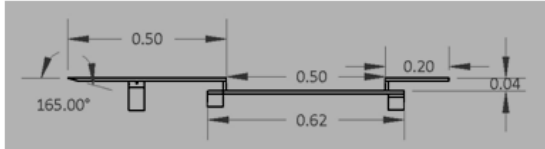


Figure 3: Dimensions of cavity model in metres.

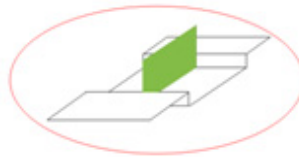


Figure 4: Location of the PIV laser sheet relative to the cavity.

3 Experimental results

3.1 Boundary layer and surface pressure measurements

The boundary layer at the leading edge of the cavity was found to conform to the 1/7 power law and hence is deduced to be turbulent. The boundary layer thickness, $\delta_{0.95}$, was found to be about 90mm. The large thickness could be attributed to both the blockage effect and the design of the leading plate before

the cavity. The pressure coefficient distribution along the centerline of the cavity floor is shown in Figure 5. The pressure gradient is slightly negative up to a x/L of ~ 0.4 . After which, there is a gradual increase of pressure towards the cavity aft. These observations are typical of an open flow configuration.

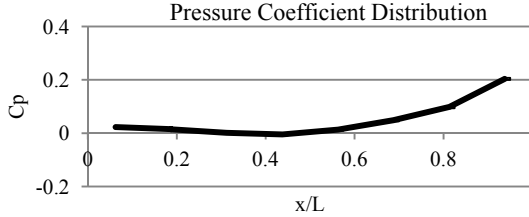


Figure 5: Pressure coefficient distribution along centerline of cavity floor.

3.2 PIV time-averaged results

The 900 independent images acquired from PIV were first averaged to obtain mean field variables. These included the mean flow field in the x and y direction, the in-plane streamlines, velocity fluctuations in the x and y direction, Reynolds shear stress, vorticity and spatial correlation. These quantities will be discussed below. Figure 6 shows the mean velocity in the x and y direction, U and V , as well as the in-plane streamlines. The contour distributions, as well as the large recirculating bubble within the cavity are typical of an open cavity configuration.

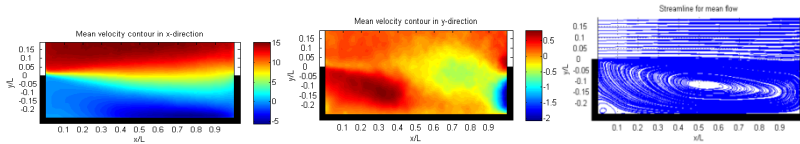


Figure 6: U (left), V (middle), in-plane streamlines (right).

Normalised velocity fluctuations for the cavity in x and y direction, $\frac{u'}{U_\infty}$ and $\frac{v'}{U_\infty}$ are shown in Figure 7 while the Reynolds shear stress, $\frac{u'v'}{U_\infty^2}$, is shown in Figure 8. In each figure, a similar study done by Ukeiley *et al.* [5] for $L/D=5.16$ at a Mach number of 0.2 is shown on the right for comparison. The general distribution of $\frac{u'}{U_\infty}$ for this study is similar to that of Ukeiley *et al.* [5] as shown in Figure 7. However, there is a region of high intensity above the cavity, especially at the top right corner of the contour plot of this study. This could be due to the thick boundary layer. If this region is ignored, a maximum value of about 0.3 is found along the lip line towards the trailing edge of the cavity. This is comparable to the maximum value of intensity found by Ukeiley *et al.* [5], which also occurs near the trailing edge of the cavity. Similar to the plots of $\frac{u'}{U_\infty}$, the two plots of $\frac{v'}{U_\infty}$ have the same distribution except for the patch of high intensity above the cavity

for this study. A maximum intensity of 0.2 is found for this study, which is comparable to the maximum value of 0.170 found by Ukeiley *et al.* [5]. The position of the maximum intensity occurs near the trailing wall of the cavity in both cases. From Figure 8, the Reynolds shear stress distribution of this study is also similar to that of Ukeiley *et al.* [5], with the maximum value occurring towards the trailing edge of the cavity. A maximum value of around 0.03 is obtained in this study while a maximum value of about 0.015 was obtained by Ukeiley *et al.* [5].

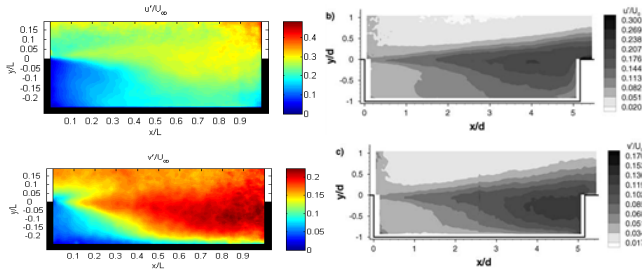


Figure 7: Contour plot of $\frac{u}{U_\infty}$ and $\frac{v}{U_\infty}$ (left: current study, right: Ukeiley *et al.* [5]).

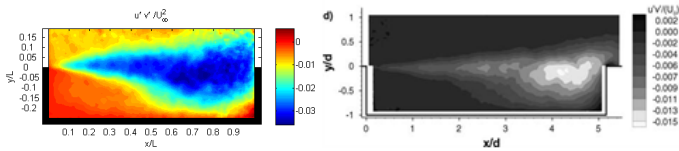


Figure 8: Contour plot of $\frac{u'v}{U_\infty^2}$ (left: current study, right: Ukeiley *et al.* [5]).

Contour plot of normalized vorticity, $\frac{\omega_z D}{U_\infty}$ (D and U_∞ , denotes respectively the cavity depth and free stream velocity) was compared against that of Ukeiley *et al.* [5] in Figure 9. Region of higher vorticity was limited to the shear layer in both cases, with some levels of vorticity spreading towards the aft section of the cavity. This is due to the high speed free-stream fluid interacting with the low speed fluid inside the cavity. Both plots have vorticity values in similar range.

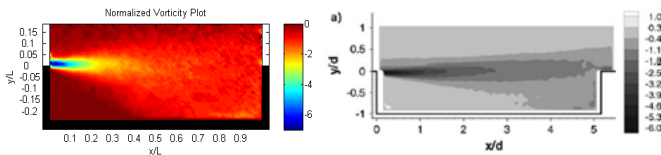


Figure 9: Contour plot of $\frac{\omega_z D}{U_\infty}$ (left: current study, right: Ukeiley *et al.* [5]).

In order to estimate the growth in length scales of coherent structures across the lip line of the cavity, two point spatial correlation coefficients of both the x and y velocity fluctuations were examined. The spatial correlation in x direction is represented by R_{uu} and the spatial correlation in y direction by R_{vv} . The spatial correlation for v' velocity is calculated as

$$R_{vv}(x_o, y_o) = \frac{\langle v'(x_o)v'(x) \rangle}{\sqrt{v'(x_o)^2}\sqrt{v'(x)^2}} \quad (1)$$

where x_o and y_o denote the reference position for x and y respectively. For this calculation, a reference point was first chosen. The velocity fluctuation at all points in an individual image was correlated to the velocity fluctuation at this reference point. The same correlation procedure was carried out for all 900 images, the result of which was averaged to give the final image. Five reference positions were chosen for both R_{uu} and R_{vv} . These 5 positions lie on the lip line of the cavity and correspond to positions where $x/L=0.1, 0.3, 0.5, 0.7$ and 0.9 . The aim of selecting these 5 positions was to track the growth of the shear layer across the lip. The results are presented in Figure 10, where the lengths of the structures were also measured and shown in cases when structures are smaller than the size of cavity.

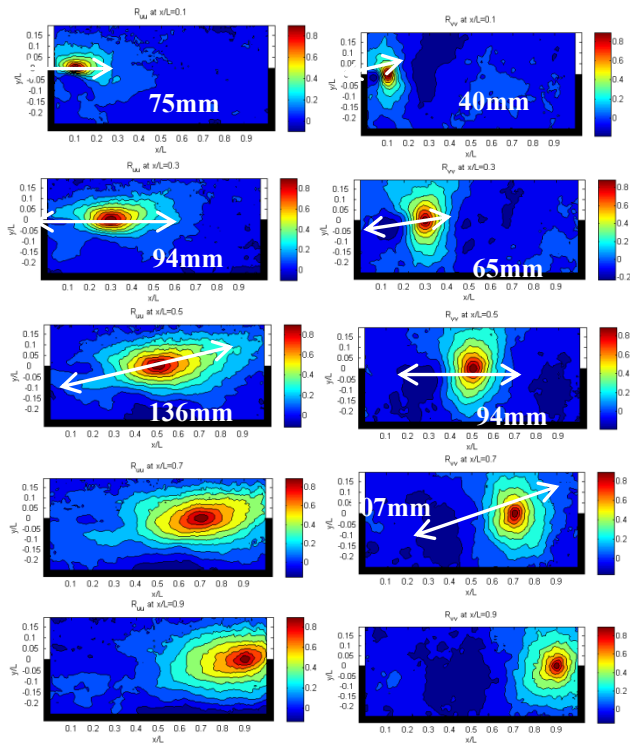


Figure 10: R_{uu} (left) and R_{vv} (right).

In R_{uu} , the length and height of the region of high positive correlation grows with increasing distance from the cavity leading edge. This is consistent with the amplification of disturbances by the shear layer to form large scale coherent structures. In R_{vv} , the correlated regions have roughly circular contours. There appears to be a distinct pattern of alternating regions of positive and negative coefficient values across the span of the cavity, shown by the red and dark blue regions. This reflects the organized nature of the coherent structures within the cavity. Again, the area of positive correlation grows across the cavity.

The velocity profiles across the shear layer as a function of x/L is shown in Figure 11. The plots indicate that the shear layer attains self-similarity beyond $x/L=0.3$. The growth in momentum thickness as shown in Figure 12 was estimated to be around 0.031. This is close to the entrainment rate of the mixing layer measured by Liepmann *et al* [6] which has $\frac{d\theta}{dx}$ value of 0.035.

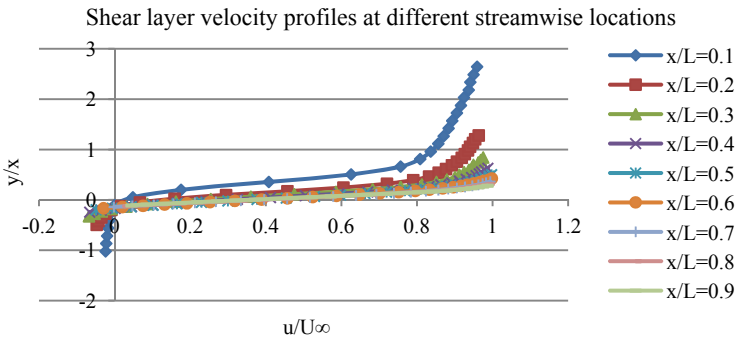


Figure 11: Velocity profiles at different streamwise locations.

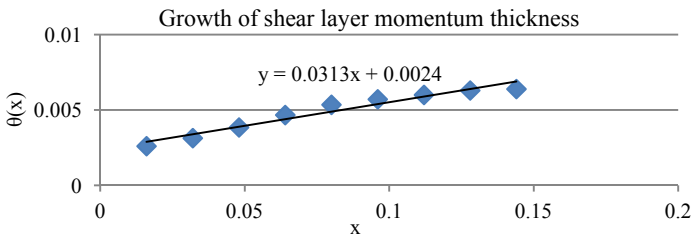


Figure 12: Growth of shear layer across the cavity lip line.

3.3 Proper Orthogonal Decomposition (POD)

3.3.1 Theory of POD

POD was first introduced in the context of turbulence by Lumley [7] as an unbiased way of extracting coherent structures from turbulent flows. It provides an empirical basis for representations of complex spatio-temporal fields that is optimal in the sense that it converges faster on average than any other representation. Detailed explanations of POD can be found in Holmes *et al.* [8]



and Delville *et al.* [9]. Sirovich [10] introduced the snapshot POD method that utilized spatially resolved but time un-correlated snapshots of the flow field like those obtained by PIV. The spatial modes associated with snapshot POD, ϕ , were assumed to have a special form in terms of the original velocity data:

$$\phi(x) = \sum_{n=1}^N a^{(n)} U_i^{(n)}(x) \quad (2)$$

where the temporal coefficients $a^{(n)}$, $n=1, \dots, N$ are to be determined. A consequential eigenvalue problem is hence deduced to solve for $a^{(n)}$:

$$C a^{(n)} = \lambda^{(n)} a^{(n)} \quad (3)$$

Flow reconstruction can then be done through the linear combination of spatial eigenfunctions with the temporal eigenfunctions as coefficients. Through POD, the spatial eigenfunctions are orthonormal and the temporal coefficients are orthogonal.

$$U_i(x) = \sum_{n=1}^N a^{(n)}(t) \phi_i^{(n)}(x) \quad (4)$$

3.3.2 Application of POD to PIV data

POD was applied to all 900 images from PIV, with the mean flow field subtracted from the images before decomposition. Figure 13 is a plot depicting the individual energy content of the modes, the sum of which contributes to 75% of the total energy in the flow. A total of about 74 modes were needed to make up 75% of the energy content in the field. The first mode has about 15.7% of the total energy. This is followed by a drop in energy for subsequent modes. Mode 2, 3 and 4 has about 7.3%, 5.6% and 4.5% of total energy respectively. For reconstruction of flow, the first 4, 7 and 14 modes are needed to recover 33%, 40% and 50% of the total energy content respectively.

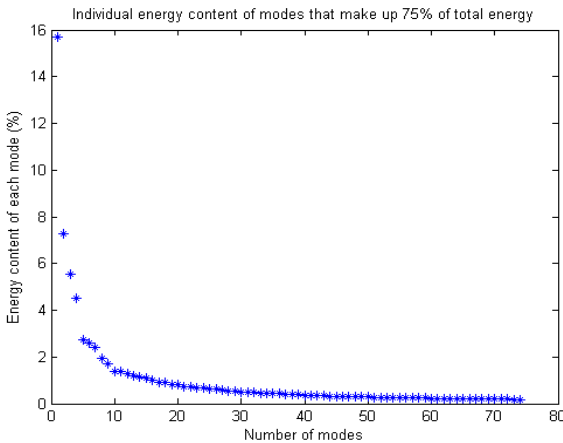


Figure 13: Individual energy content of modes.

The first 5 spatial modes in the y direction are shown in Figure 14. These plots reveal the structures that are contributing to each mode. From the spatial modes, the length scales of the structures were estimated, where clear structures could be identified. This is indicated by the white arrows in modes 2 to 5. From the figure, mode 1 has a structure that stretches through the entire cavity. Hence, the length-scale is taken to be the length of the cavity, 160mm. Mode 2 and mode 3 both have a length scale of about 114mm while mode 4 has a length scale of about 100mm and mode 5 has a length scale of about 83mm. The decrease in the length scale of structure with the increase in the mode number is expected as smaller structures contribute to a lesser percent of the total energy in the flow.

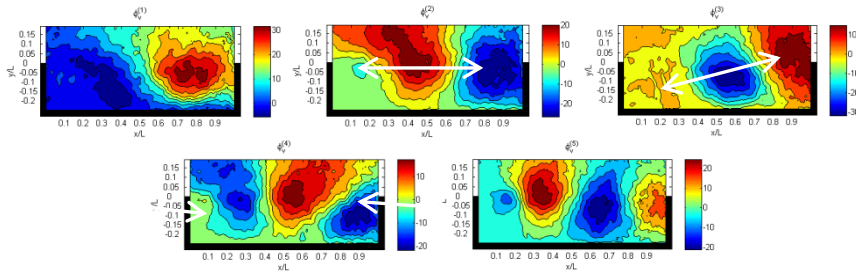


Figure 14: Plots of first 5 $\phi_V^{(n)}$.

The in-plane streamlines of modes 1 to 3 were also plotted in Figure 15. These streamlines represent the contribution of the modes in both the x and y direction. Inspection of the in-plane streamlines seems to indicate the flapping of the shear layer. One could deduce this fact from the super position of these modes onto the mean in-plane streamlines profile as shown in Figure 6 and eqn (4). Mode one and two indicated a flow structure of the closed cavity type while mode three indicated the possibility of a large structure ejecting from the aft of the cavity.

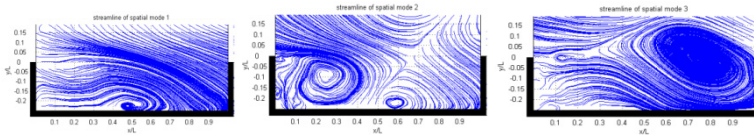


Figure 15: In-plane streamlines of individual spatial mode.

3.3.3 Reconstruction of flow with first four POD modes

Reconstruction of flow was done with the first 4 modes to see how well these modes can estimate the original mean flow field as well as whether the turbulent noise due to the thick boundary layer can be decoupled. The mean quantities are recalculated from the reconstructed field. Figure 16 shows the mean velocity in the x and y direction, U and V, as well as the in-plane streamlines. When comparing Figure 16 with Figure 6, it was observed that both U and V, and

hence the in-plane streamlines, have been successfully reconstructed. Reconstructed normalised velocity fluctuations in x and y direction, $\frac{u'}{U_\infty}$ and $\frac{v'}{U_\infty}$, are shown in Figure 17 while the reconstructed Reynolds shear stress, $\frac{u'v'}{U_\infty^2}$, is shown in Figure 18. In the contour plot of $\frac{u'}{U_\infty}$ and $\frac{v'}{U_\infty}$, it was observed that the region of high intensity above the cavity that was present in Figure 7 has now disappeared. This implies that we could decouple the turbulent background noise from the results. The general distribution of velocity fluctuations here is about the same as the original flow field in both x and y direction. For $\frac{u'}{U_\infty}$, a maximum value of 0.25 was obtained, which is comparable to the original value of 0.3. For $\frac{v'}{U_\infty}$, a maximum intensity of about 0.14 was obtained, which is slightly lower than the original value of 0.2. This loss of energy was expected as the background turbulent noise has been filtered by the POD procedure. In the contour plot of $\frac{u'v'}{U_\infty^2}$, the maximum value of 0.03 and its position is similar to the original flow shown in Figure 8. However, the intensity at the leading edge is lower here than in the original flow.

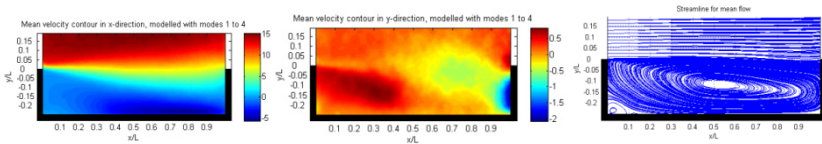


Figure 16: Contour of reconstructed U (left), V (middle) and in-plane streamlines (right), using the first 4 modes.

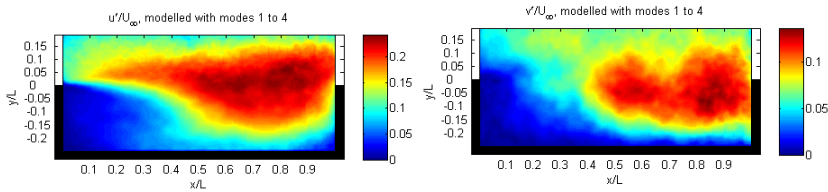


Figure 17: Contour plot of $\frac{u'}{U_\infty}$ (left) and $\frac{v'}{U_\infty}$ (right), modelled by first 4 modes.

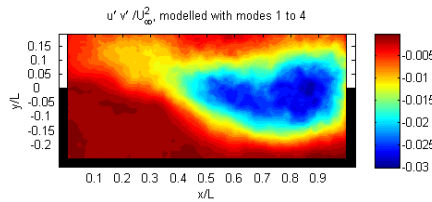


Figure 18: Contour plot of $\frac{u'v'}{U_\infty^2}$, modelled by first 4 modes.

Overall, it seems that the first 4 modes were able to replicate the mean flow field to a fairly accurate extent. This is an important feature of POD since using less number of modes to model the flow field accurately means that cost of computation can be reduced or that flow control studies could be carried out more efficiently.

4 Conclusion

The present work has made use of several data reduction tools to post process PIV data of an open cavity with $L/D=4$. The shear layer which grows across the cavity was found to attain self-similarity in the velocity profiles beyond $x/L=0.3$. The rate of growth in momentum thickness of this shear layer was estimated to be around 0.031, a value close to the entrainment rate of a turbulent mixing layer. Time-averaged quantities of the flow revealed the mean flow characteristics within the cavity while spatial correlations of velocity fluctuations indicated the presence of organized coherent structures which grew across the shear layer of the cavity. POD was applied to PIV data to derive the structures responsible for the different modes of flow. From the POD results, the first four modes were used to reconstruct the flow. This filtering process could remove the turbulent background noise successfully.

References

- [1] Kook, H., Mongeau, L., Brown, D.V. & Zorea, S.I., *Analysis of the interior pressure oscillations induced by flow over vehicle openings*. Noise Control Engineering Journal, **45**, pp. 223-234, 1997.
- [2] Gharib, M. & Roshko, A., *The effect of flow oscillations on cavity drag*. Journal of Fluid Mechanics, **177**, pp. 501-30, 1987.
- [3] Rockwell, D. & Naudascher, E., *Review-self-sustaining oscillations of flow past cavities*. Transactions of the ASME. Journal of Fluids Engineering, **100**, pp. 152-65, 1978.
- [4] Plentovich, E.B., *Experimental Cavity Pressure Measurements at Subsonic and Transonic Speeds*. NASA Technical Paper 3358. 1993.
- [5] Ukeiley, L. & Murray, N., *Velocity and surface pressure measurements in an open cavity*. Experiments in Fluids, **38**(5), pp. 656-671, 2005.
- [6] Liepmann, H.W. & Laufer, J., *Investigation of free turbulent mixing*, National Advisory Committee for Aeronautics: Washington, DC, United States, 1947.
- [7] Lumley, J., *The Structure of Inhomogeneous Turbulent Flows*. Atmospheric Turbulence and Wave Propagation, Moscow: Nauka, 1967.
- [8] Holmes, P., Lumley, J. & Berkooz, G., *Turbulence, Coherent Structures, Dynamical Systems and Symmetry*, Cambridge, England: Cambridge University Press, 1996.
- [9] Delville, J., Cordier, L. & Bonnet, J.P., *Large-Scale-Structure Identification and Control in Turbulent Shear Flows*, Springer Berlin / Heidelberg, pp. 199-273, 1998.



- [10] Sirovich, L., *Turbulence and the dynamics of coherent structures. I. Coherent structures*. Quarterly of Applied Mathematics, **45**, pp. 561-70, 1987.

